Four-Body Reaction Dynamics: Complete Correlated Fragment Measurement of the Dissociative Photodetachment Dynamics of O_8^-

Todd G. Clements and Robert E. Continetti*

Department of Chemistry and Biochemistry, University of California–San Diego, 9500 Gilman Drive, La Jolla, California 92093-0340

(Received 5 March 2002; published 1 July 2002)

The four-body dissociative photodetachment (DPD) dynamics of O_8^- were studied using photoelectron photofragment coincidence (PPC) spectroscopy. All four neutral photofragments were measured in coincidence with the photodetached electron, yielding a five-body kinematically complete experiment. Velocity and angular correlations for DPD of O_8^- are presented and compared to those for O_6^-. The DPD dynamics and energetics of O_8^- are found to be similar to those of O_4^- and O_6^- implying that the additional solvating O_2 molecules act essentially as spectators, but exhibit inequivalent kinematic behavior implying asymmetric solvation.

DOI: 10.1103/PhysRevLett.89.033005 PACS numbers: 33.80.Gj, 33.80.Eh, 34.50.–s, 36.40.–c

In recent years, there has been an increase in both theoretical and experimental studies of many-body dynamics. This is a result of increased computational power available to model the multidimensional potential surfaces of many-body systems as well as the advent of new experimental methods for detecting multiple particles in coincidence during a many-body breakup. At the chemical level (as opposed to the subatomic particle level), the study of three-body processes has dominated the many-body literature. Reviews of three-body dissociation dynamics from many atom systems [1] and coincidence techniques which can be used to study three-body breakups [2] have appeared in recent literature. As a natural progression from three-body dynamics, studies of four-body systems have emerged. Experiments such as the double ionization of helium by electron impact followed by detection of two electrons and the He^{+2} fragment, or $(e, 3e)$ reactions, represent some of the first work on a chemical level four-body dynamics [3–5]. Owing to the difficulty of multibody detection, in these experiments as in many previous three-body experiments, all but one particle is detected, and the energy of the remaining particle is determined by knowledge of the identity of the fragments coupled with conservation of momentum. More recently, Müller and co-workers have built a multiple fragment coincidence spectrometer and developed data analysis algorithms which can distinguish between two-, three-, and four-body dissociation, although only three-body dissociations have been reported until now [6,7].

In this Letter, results from experiments employing photoelectron photofragment coincidence (PPC) spectroscopy on the four-body dissociative photodetachment (DPD) of O_8^- are reported. PPC spectroscopy allows for detection of all four neutral O_2 fragments that arise from DPD of O_8^- in coincidence with the photodetached electron, providing a kinematically complete five-body experiment. From these experiments, insight into the energetics and four-body dissociation dynamics of the O_8 neutral is obtained.

Previous experimental investigations on the homogeneous cluster ions $(O_2)_n^-$ include mass spectroscopy [8], photoelectron spectroscopy [9–11], matrix isolation [12], and PPC spectroscopy [13–15] experiments. It is generally believed that clusters with $n > 2$ consist of an O_4^- core with a delocalized electron surrounded by loosely bound solvating O_2 molecules. Since O_4^- is stabilized by 0.45 eV relative to O_2^-, and successive O_2 molecules stabilize the cluster by less than 0.11 eV each, the presence of an O_4^- core is supported by the sudden change in solvation energy after formation of O_4^- [8]. Aquino *et al.* studied O_4^- via *ab initio* methods and concluded that the diffuse nature of the a_g molecular orbital formed from the antibonding π_g orbitals in the oxygen subunits plays an important role in the bonding of O_4^- [16]. Additionally, PPC experiments on the three-body DPD dynamics of O_6^- show that the third O_2 molecule essentially acts as a spectator to an O_4^- core with remarkably similar dynamics to those seen in the DPD of O_4^- [15].

The PPC spectrometer employed for these studies has been described in detail elsewhere and will only be briefly reviewed here [17]. Cold anions are made in a pulsed (1 kHz) free jet expansion of neat O_2 intersected by a 1 keV electron beam. Anions are extracted and accelerated to 4–6 keV and mass selected by time of flight. Anions with $m/e = 96$ (O_6^-) or 128 (O_8^-) are intersected with the third harmonic (258 nm) of a linearly polarized Ti:sapphire laser (Clark MXR, Inc.) providing a fluence of $\sim(1-3)$ mJ/cm^2 per 1.2 ps FWHM pulse. The photodetached electron is detected by one of two opposed microchannel-plate-based time- and position-sensitive detectors positioned orthogonal to both the ion and laser beams. The time and position information is used to calculate the center-of-mass (c.m.) velocity vector and thus the electron kinetic energy (eKE) and correct for the Doppler shift that arises from the use of a fast ion beam. This detector has been shown to have a resolution of $\sim 5\%$ $\Delta E/E$ at 1.3 eV and is calibrated using the photodetachment of I^- and O_2^-.

Recoiling neutral fragments travel over a 104 cm flight path and impinge on a microchannel plate assembly. The electron cloud produced by this assembly is detected by a four-quadrant time- and position-sensitive delay line detector, where each quadrant is capable of detecting up to two particles per dissociation event as long as they are separated by 10 ns. Thus, given the correct dissociation kinematics, four neutral particles can be detected for a single dissociation event. Generally, events with a lower kinetic energy release (E_T) will be discriminated against more than events with a high E_T since these events spread out on the detector face and can overcome the 10 ns dead time. Despite this kinematically complete detection of the neutral particles, the four-body mass equations cannot always be solved exactly since many different mass combinations can lead to the same momentum partitioning. For example, if two fragments recoil along the x axis and two fragments recoil along the y axis, the mass ratio between the two sets of fragments cannot be determined. As a result, in the current calculations all photofragments from DPD of O_8^- are assigned mass 32 amu, corresponding to dissociation to four O_2 molecules. At this photon energy, this is the only energetically available pathway for this system. Subtracting the electron affinity of O_2 (0.451 eV) [18] and the successive heats of solvation for O_2^- by O_2 (Ref. [8]) from the photon energy, 4.80 eV, leaves $4.80 - 0.451 - 0.74 = 3.61$ eV of available energy assuming production of $4O_2(X^3\Sigma_g^-) + e^-$ with no internal excitation. Formation of $2O_2(X^3\Sigma_g^-) + O_3 + O + e^-$ would require an additional 4.06 eV of energy [19] and is not accessible at this wavelength. Once the masses are assigned, momenta and E_T are easily calculated from the time and position of arrival for each photofragment. For the two-body photodissociation of O_2^-, this detector has been shown to have a resolution of $\sim 10\%$ $\Delta E/E$ at 0.7 eV.

Each analyzed event is required to consist of four neutral photofragments and a single electron. The number of neutral particles analyzed was selected by gating on the total charge observed from the microchannel plates, which is well-resolved for one, two, three, and four neutral particles. In order to reduce false coincidences, conservation of momentum is checked for each event. The false coincidence rate for these experiments derives from the detector efficiency and the count rate, and is calculated in a similar manner as done previously for three-body experiments [17]. A false coincident rate of approximately 8% is obtained for an event rate of 0.08 dissociations per laser shot.

Figure 1 shows the photoelectron-photofragment correlation spectrum, $N(E_T, e\mathrm{KE})$ for DPD of O_8^- at 258 nm. This figure represents a two-dimensional histogram of the correlated E_T and eKE for each dissociation event. The one-dimensional E_T and eKE spectra are generated by integrating the correlation spectrum over the complementary variable. As seen by Johnson and co-workers at 355 nm, the photoelectron spectrum of O_8^- is broad and shows no vibrational resolution [10]. Through conservation of energy, a diagonal line can be drawn, labeled as A, representing the maximum energy available for translation in the photoproducts. The placement of this line at 3.61 eV is given by the energetic limitations mentioned above. Energetic limits for dissociation channels yielding one or more O_2 products in the $a^1\Delta_g$ or $b^1\Sigma_g^+$ excited electronic states are also shown in Fig. 1.

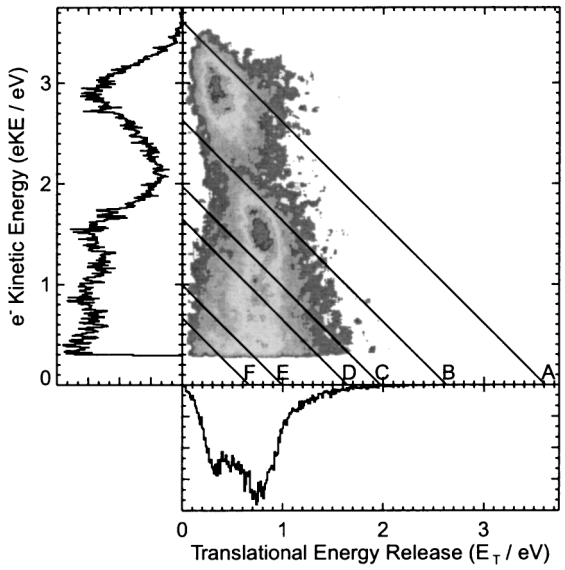

FIG. 1. Photoelectron-photofragment correlation spectrum, $N(E_T, e\mathrm{KE})$, for the dissociative photodetachment of O_8^- at 258 nm. The diagonal line marked (A) represents the maximum translational energy release for production of $4O_2(X^3\Sigma_g^-) + e^-$. Successive lines mark energetic limitations for production of an electron and (B) $3O_2(^3\Sigma_g^-) + O_2(a^1\Delta_g)$, ($C$) $3O_2(^3\Sigma_g^-) + O_2(^1\Sigma_g^+)$, ($D$) $2O_2(X^3\Sigma_g^-) + 2O_2(a^1\Delta_g)$, ($E$) $2O_2(X^3\Sigma_g^-) + O_2(a^1\Delta_g) + O_2(b^1\Sigma_g^+)$, and ($F$) $O_2(X^3\Sigma_g^-) + 3O_2(a^1\Delta_g)$.

The $N(E_T, e\mathrm{KE})$ spectrum and the corresponding $N(E_T)$ and $N(e\mathrm{KE})$ spectra for O_8^- at 258 nm bear a striking resemblance to those for O_4^- at 266 nm [13], as well as O_6^- at 258 nm (not shown), implying similar partitioning of energy in all three systems. As in O_4^- and O_6^-, DPD forming all ground electronic state O_2 products [between lines $1(A)$ and $1(B)$] occurs with a low neutral molecule translational energy release, peaking at $E_T = 0.35$ eV for DPD of O_8^-. However, DPD producing excited state O_2 fragments, such as $3O_2(^1\Sigma_g^-) + O_2(a^1\Delta_g) + e^-$ seen below line $1(B)$, occurs with a higher neutral molecule translational energy release, peaking at $E_T = 0.75$ eV, implying more steeply repulsive potential energy surfaces correlated with production of $O_2(a^1\Delta_g)$.

The correlation spectra for both O_4^- and O_6^- revealed diagonal ridges which correspond to DPD on vibrationally adiabatic repulsive curves correlating to different vibrational states of the O_2 products [13,14]. In the case of O_6^-, however, these ridges were broader and less prominent due to the presence of the third O_2. For O_8^-, no diagonal features were observed. The similarity of the correlation

spectrum for O_8^- to those of O_6^- and O_4^- implies that the lack of diagonal features is a result of rotational excitation among the four O_2 products.

The effect of the two solvating O_2 molecules on the dissociation dynamics can be probed through examination of velocity and angular correlations between the dissociating fragments. Figure 2 shows the three-body molecular frame differential cross sections (MF-DCS) for the dissociation of O_8. These types of figures have previously been used to examine the dissociation dynamics of three-body systems, such as O_6^- (Ref. [15]) and $O^-(H_2O)_2$ (Ref. [20]). The plots are constructed by projecting the velocity vectors for each dissociation event onto the same plane, on an event-by-event basis. In the case of a four-body dissociation, the three vectors do not necessarily lie in a plane, although the planarity assumption holds well for any three fragments from DPD of O_8 due to the small velocities of the slowest two particles. One particle is chosen as a reference particle, and its velocity distribution is plotted along the x axis. The velocity of the second particle is then plotted on the lower half of the plot, relative to the reference particle. The velocity of the third particle is plotted similarly on the upper half of the plot. In the case of O_8, where four photofragments are produced with the same mass, the relative velocity of each of the fragments is used as the sorting criteria for each event. Given the dynamics of O_8, where two fragments recoil with moderate kinetic energy, and two fragments recoil with low kinetic energy, this velocity sorting method at least allows for comparison of the velocity and angular distributions between the fastest and the slowest sets of fragments. Although the MF-DCS gives only velocity and angular correlations for three particles at once, insight into the four-body dynamics can be obtained by examining a series of these plots with different reference particles. Thus Fig. 2 shows four MF-DCSs for O_8, each plot employing a different velocity-sorted fragment as the reference particle.

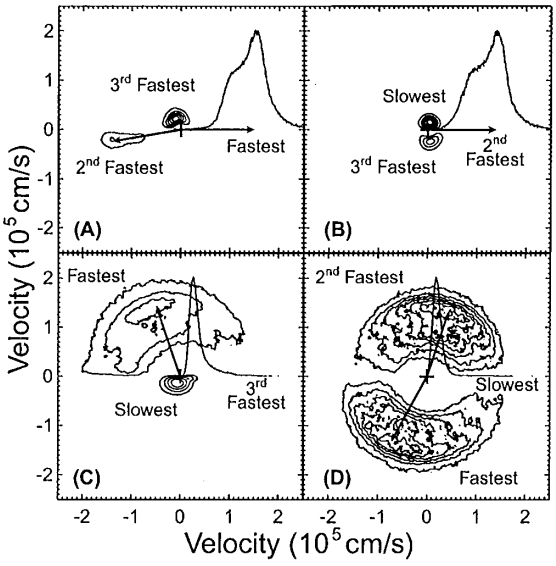

FIG. 2. Molecular frame differential cross sections (MF-DCS) for the dissociative photodetachment of O_8^-. The velocity of the reference particles is plotted along the x axis and the velocity of two other particles is plotted relative to the reference particle, as discussed in the text. The labels fastest, second fastest, third fastest, and slowest indicate the relative velocity of each fragment sorted on an event-by-event basis. In frame (C), the upper half of the plot was scaled by a factor of 10 to make the contours visible.

The MF-DCS plots for O_8 show the dominance of two fast particles during the dissociation. Figure 2(A) shows the velocity correlation for the fastest three fragments, and resembles the MF-DCS seen for O_6 at 258 nm where the two fastest fragments recoiled at nearly 180°, and the slowest fragment carried very little momentum [15]. As in the case of DPD of O_6^- at 258 nm, the fastest particles exhibit two peaks in the velocity distribution. The lower velocity peak along the x axis is a result of dissociation to all ground state products, $4O_2(X^3\Sigma_g^-) + e^-$, and the higher velocity peak corresponds to production of electronically excited oxygen fragments, $3O_2(X^3\Sigma_g^-) + O_2(a^1\Delta_g$ or $b^1\Sigma_g^+) + e^-$. Figure 2(B) shows that the two slowest fragments recoil with a wide range of angles relative to the second fastest fragment. In Fig. 2(C), the two slowest fragments are seen to recoil slightly backwards relative to one another, although the small recoil velocities of these two particles make angular determinations more difficult. Figure 2(D) indicates that the two fastest particles recoil with a broad distribution of angles relative to the slowest particle. The maxima of the contours of the faster particles occur at $\sim 15°-20°$ from perpendicular to the recoil of the slowest particle.

Figure 3 shows a direct comparison between the momenta of the fastest, second fastest, and slowest fragments from DPD of O_6^- to the equivalent fragments from DPD of O_8^-. This figure shows that the fastest O_2 fragments in each dissociation have almost identical momentum distributions, while the momentum distributions for the slower particles differ noticeably. The striking similarity between the fastest fragments in the DPD of O_6^- and O_8^- imply that these fragments, from the O_4^- core, do not interact significantly with the additional solvating O_2 molecules. However, the second fastest fragment shows noticeable slowing in O_8 relative to O_6. This may arise from momentum transfer to the solvent O_2 molecules implying asymmetric solvation of the O_4^- core. This type of asymmetric solvation has been seen in $I_2^-(CO_2)_n$ clusters [21] and results from a slight polarization of the anionic core by the first solvated molecule(s). Also notable in this figure is the higher-momentum tail on the third fastest O_2 fragment, and the inequivalent peak position and shape for the two slowest O_2 fragments from O_8^- DPD. The difference in momentum distributions for the two fragments is consistent with a structural inequivalence in the nascent neutral complex.

This data is interpreted with a model very similar to that proposed for O_6^- [15]. In this model, the two fast

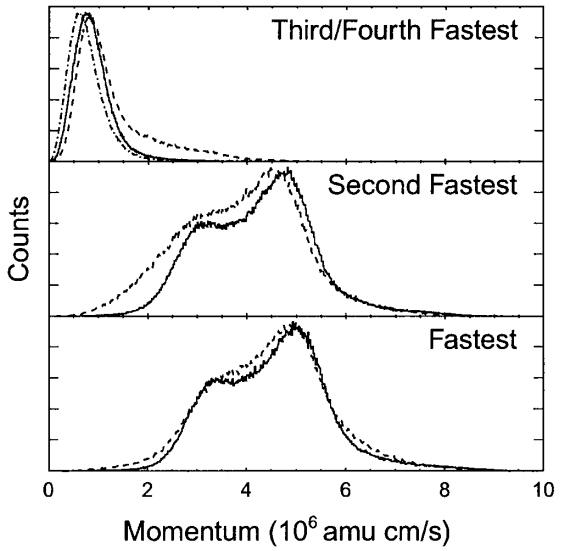

FIG. 3. Momentum distributions for the neutral O_2 products of O_6^- (solid) and O_8^- (dashed) DPD. The fastest, second fastest, and slowest O_2 products from O_6^- DPD are compared with the fastest, second fastest, and two slowest O_2 products from O_8^- DPD, respectively.

fragments arise from the dissociation of the O_4 core of the O_8 molecule, and the two slow fragments act essentially as spectators during this dissociation. A structure where the two O_2 molecules solvate O_4^- on the same side of the O_4^- plane may give rise to inequivalent O_2 fragments. In the case of O_6^-, it was not possible to rule out a structure where the three O_2 molecules formed a linear complex, and the low momentum transfer to the third O_2 molecule was due to the simultaneous ejection of the end O_2 molecules, leaving the third at the center of mass for the system. This structure, with the fourth O_2 molecule solvating the linear O_6^- core, could also explain the inequivalence of the two slowest O_2 fragments. From the current data, it is not possible to assign either structure to the O_8^- cluster; however, the energetic arguments discussed above strongly argue for the O_4^- core.

In conclusion, this work has demonstrated the feasibility of performing four-body correlated neutral fragment detection. The results obtained for DPD of O_8^- are consistent with the results obtained for DPD of O_4^- and O_6^-. Correlated four-neutral plus electron energy spectra reveals that DPD to all ground state products $O_8^- + h\nu \rightarrow 4O_2(X^3\Sigma_g^-) + e^-$ occurs to a repulsive region of the potential surface while production of electronically excited O_2 products occurs to more steeply repulsive surfaces, resulting in higher translational energy release. The dynamics of the dissociative photodetachment of O_8^- are very similar to those for O_6^-. Dissociation releases most of the available E_T to two of the O_2 fragments, and the remaining two O_2 fragments act as spectators during the dissociation. Acquisition of four-body dissociation data on larger molecular clusters provides further insight into the transition from gas-phase to condensed-phase dynamics and represents a new and exciting area for experimental and theoretical investigation.

This work was supported by the Air Force Office of Scientific Research under Grant No. F49620-00-1-0010.

*Corresponding author.
Email address: rcontinetti@ucsd.edu

[1] C. Maul and K.-H. Gericke, Int. Rev. Phys. Chem. **16**, 1 (1997).
[2] R. E. Continetti, Annu. Rev. Phys. Chem. **52**, 165 (2001).
[3] C. Schroter, B. El Marji, A. Lahmam-Bennani, A. Duguet, M. Lecas, and L. Spielberger, J. Phys. B **31**, 131 (1998).
[4] A. Dorn, A. Kheifets, C. D. Schroter, B. Najjari, C. Hohr, R. Moshammer, and J. Ullrich, Phys. Rev. Lett. **86**, 3755 (2001).
[5] A. Kheifets, I. Bray, A. Lahmam-Bennani, A. Duguet, and I. Taouil, J. Phys. B **32**, 5047 (1999).
[6] M. Beckert and U. Müller, Eur. Phys. J. D **12**, 303 (2000).
[7] M. Braun, M. Beckert, and U. Müller, Rev. Sci. Instrum. **71**, 4535 (2000).
[8] K. Hiraoka, J. Chem. Phys. **89**, 3190 (1988).
[9] C. C. Han and M. A. Johnson, Chem. Phys. Lett. **189**, 460 (1992).
[10] M. J. DeLuca, H. Chau-Chung, and M. A. Johnson, J. Chem. Phys. **93**, 268 (1990).
[11] D. H. Paik, T. M. Bernhardt, K. Nam Joon, and A. H. Zewail, J. Chem. Phys. **115**, 612 (2001).
[12] G. V. Chertihin and L. Andrews, J. Chem. Phys. **108**, 6404 (1998).
[13] K. A. Hanold and R. E. Continetti, Chem. Phys. **239**, 493 (1998).
[14] K. A. Hanold, A. K. Luong, and R. E. Continetti, J. Chem. Phys. **109**, 9215 (1998).
[15] A. K. Luong, T. G. Clements, and R. E. Continetti, in *Imaging in Chemical Dynamics,* edited by A. G. Suits and R. E. Continetti (American Chemical Society, Washington, DC, 2001), p. 312.
[16] A. J. A. Aquino, P. R. Taylor, and S. P. Walch, J. Chem. Phys. **114**, 3010 (2001).
[17] K. A. Hanold, A. K. Luong, T. G. Clements, and R. E. Continetti, Rev. Sci. Instrum. **70**, 2268 (1999).
[18] M. J. Travers, D. C. Cowles, and G. B. Ellison, Chem. Phys. Lett. **164**, 449 (1989).
[19] M. W. Chase, Jr., C. A. Davies, J. R. Downy, Jr., D. J. Frurip, R. A. McDonald, and A. N. Syverud, *JANAF Thermochemical Tables* (American Institute of Physics, New York, 1985).
[20] T. G. Clements, A. K. Luong, H.-J. Deyerl, and R. E. Continetti, J. Chem. Phys. **114**, 8436 (2001).
[21] A. Sanov, T. Sanford, S. Nandi, and W. C. Lineberger, J. Chem. Phys. **111**, 664 (1999).